

Guided Policy Search Based Control of a High Dimensional Advanced Manufacturing Process

Amit Surana
Kishore Reddy
Matthew Siopis

SURANAA@UTRC.UTC.COM
REDDYKK@UTRC.UTC.COM
SIOPISMJ@UTRC.UTC.COM

Raytheon Technologies Research Center, 411 Silver Lane, East Hartford, CT, 06118, USA

Abstract

In this paper we apply guided policy search (GPS) based reinforcement learning framework for a high dimensional optimal control problem arising in an additive manufacturing process. The problem comprises of controlling the process parameters so that layer-wise deposition of material leads to desired geometric characteristics of the resulting part surface while minimizing the material deposited. A realistic simulation model of the deposition process along with carefully selected set of guiding distributions generated based on iterative Linear Quadratic Regulator is used to train a neural network policy using GPS. A closed loop control based on the trained policy and in-situ measurement of the deposition profile is tested experimentally, and shows promising performance.

Keywords: Reinforcement learning, Direct policy search, Additive manufacturing control

1. Introduction

In this paper we apply guided policy search (GPS) a deep reinforcement learning (RL) approach for a high dimensional optimal control problem in an additive manufacturing (AM) process. Deep RL has recently shown unprecedented success in dealing with high dimensional problems [Mnih et al. \(2015, 2016\)](#); [Silver et al. \(2018\)](#); [Lillicrap et al. \(2015\)](#); [Duan et al. \(2016\)](#). Guided policy search (GPS) [Levine and Koltun \(2013, 2014\)](#); [Levine and Abbeel \(2014\)](#); [Levine et al. \(2016\)](#) is a direct policy search method which uses a neural network (NN) to parameterize the policy, and transforms the policy search into a supervised learning problem, where the training set (which guides the policy search to regions of high reward) is generated by simple trajectory-centric algorithms. It employs a regularized importance sampled policy optimization to enable stable and efficient training.

The problem considered in this paper comprises of controlling the process parameters during cold spray (CS), a metal AM process [Yin et al. \(2018\)](#). Specifically, the goal is to control the spray nozzle motion, so that layer-wise deposition of material leads to desired geometric characteristics of the resulting part surface while minimizing the material deposited. The relationship between the surface profile growth and nozzle motion is governed by a time dependent nonlinear partial differential equation (PDE). We discretize the PDE in space/time to obtain a finite dimensional nonlinear input-output system, and use a nonlinear optimization framework to calibrate the CS model parameters based on the experimental data. The NN policy is trained using GPS on the calibrated model using a carefully selected set of guiding distributions generated based on iterative Linear Quadratic Regulator. In order to ensure that the errors made by NN controller during layer deposition do not propagate to successive layers, we use suitable domain randomization. Closed loop control based on the trained NN policy was implemented in a lab setup with feedback from laser displacement sensor which measures the surface profile in real time during deposition. The experimental studies show a material saving of upto 35% compared to the state-of-the-art methods used for process parameter selection in the CS applications.

Related Work: Currently, the process parameter optimization in AM is done offline which does not account for in process uncertainties/disturbances. The need for in-situ monitoring, machine learning and closed loop control has been recognized as a key enabler to improve process repeatability/reliability [Tapia and Elwany \(2014\)](#); [Everton et al. \(2016\)](#); [Qi et al. \(2019\)](#). Specifically, in the CS context, [Chakraborty et al. \(2017\)](#) apply a model predictive control approach in simulations. We use a similar model/setup but employ a RL framework, and provide an experimental demonstration.

2. Cold Spray Control Problem

Cold spray (CS) is an AM process in which powder particles (typically 10 to 50 micron) are accelerated to very high velocities (200 to 1000 m/s) by a supersonic compressed gas jet at temperatures well below their melting point and then deposited on the surface to build new parts or repair structural damages such as cracks and unwanted indentations [Yin et al. \(2018\)](#). CS is a multi-scale process with complex physics [Wang et al. \(2015\)](#), making it challenging to optimize the process parameters which result in desired part properties. Additionally, the nozzle motion relative to part/defect geometry needs to be programmed to achieve desired surface deposition profile. Currently, this is accomplished by manual trial and error per part, and often results in a conservative solution leading to excess material deposition which needs to be eventually machined out to meet the required geometric tolerances. Moreover, the nozzle motion once programmed remains fixed, and is not adapted to account for any process variations/disturbances during the operation. Such an approach of overbuilding could lead to a significant loss of expensive material.

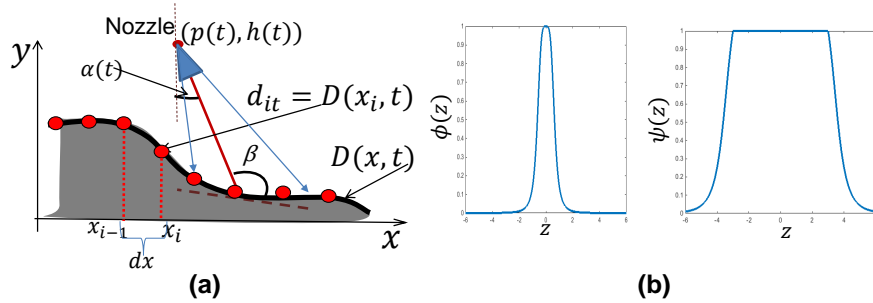


Figure 1: Cold spray model.

The focus of our work is to develop a framework for feedback control of nozzle motion that minimizes the material wastage while achieving desired surface profile. While detailed CS models are highly complex, for our control development purposes it suffices to use a reduced order model described in [Chakraborty et al. \(2017\)](#) which captures the impact of nozzle motion/spray behavior on the dynamics of deposition process at a macroscopic scale. Let $p(t)$, $h(t)$ and $\alpha(t)$ be the spray nozzle's, position and orientation as a function of time, respectively, see Fig. 1a. Then the surface height profile $D(x, t)$ ($x \in \mathbb{R}$) evolution is governed by a nonlinear integro-differential equation,

$$\frac{\partial D(x, t)}{\partial t} = \int_0^T \phi(\tan \beta(t) - \tan \alpha(t)) \psi \left(\frac{\tan \beta(t) - \frac{\partial}{\partial x} D(x, t)}{1 + \tan \beta(t) \frac{\partial}{\partial x} D(x, t)} \right) dt, \quad (1)$$

where, $\tan \beta(t) = \frac{x-p(t)}{h(t)-D(x,t)}$ and the functions

$$\phi(z) = 1 - \left(1 + \frac{\rho}{z^2}\right)^{-1}, \quad \psi(z) = \frac{1}{c} \left(0.5 + \frac{\text{atan}(-a \max(|z/b|^\kappa, 1))}{\pi}\right),$$

capture the distribution of particles in the spray cone and the nozzle efficiency, respectively (see Fig. 1b). We will denote by $\mathbf{p} = (\rho, a, b, c, \kappa)'$ as the model parameter vector, where \prime denotes the vector transpose. In above we have restricted to a one-dimensional model, as often in applications the part is rotated while nozzle motion is confined along the axis of rotation, see Sec. 4.

The space-time discretization of Eqn. (1) leads to a discrete time nonlinear input-output system

$$\mathbf{s}_{t+1} = \mathbf{f}(\mathbf{s}_t, \mathbf{u}_t; \mathbf{p}), \quad (2)$$

where, $\mathbf{s}_t = (\mathbf{d}'_t, p_t, h_t, \alpha_t)'$ is the system state, $\mathbf{u}_t = (v_t^x, v_t^h, \omega_t)'$ are the control inputs, and

$$\mathbf{f}(\mathbf{s}_t, \mathbf{u}_t) = \begin{pmatrix} d_{1t} + g_1(\mathbf{d}_t, p_t, h_t, \alpha_t; \mathbf{p})dt \\ \vdots \\ d_{N_d t} + g_{N_d}(\mathbf{d}_t, p_t, h_t, \alpha_t; \mathbf{p})dt \\ p_t + v_t^x dt \\ h_t + v_t^h dt \\ \alpha_t + \omega_t dt \end{pmatrix}. \quad (3)$$

Here, $\mathbf{d}_t = (d_{1t} \cdots d_{N_d t})'$ is the vector of discretized surface height profile $D(x, t)$, with d_{it} being the surface height at the spatial location $x_i = x_0 + (i - 1)dx, i = 1, \cdots, N_d$ and N_d is the number of discretized cells of size dx , see Fig. 1a. We assume a kinematic model of the nozzle motion, so that the nozzle position/orientation can be controlled by changing its linear v_t^x, v_t^h and angular ω_t speeds, respectively. g_i represent the discretization of the integral term appearing in the Eqn. (1).

Given initial condition $\mathbf{s}_0 = (\mathbf{d}'_0, p_0, h_0, \alpha_0)'$, the objective is to determine control sequence $\mathbf{u}_t = (v_t^x, v_t^h, \omega_t)'$, $t = 1 \cdots, T$ such that the final surface profile matches a desired profile \mathbf{d}_f ,

$$\min_{\mathbf{u}_1, \dots, \mathbf{u}_T, T} \sum_{t=1}^{T-1} c(\mathbf{s}_t, \mathbf{u}_t) + c_e(\mathbf{s}_T), \quad (4)$$

where, $c_e(\mathbf{s}_T) = \|\mathbf{d}_T - \mathbf{d}_f\|^2$ is the terminal cost, and $c(\mathbf{s}_t, \mathbf{u}_t) = w_0 + w_1(v_t^x)^2 + w_2(v_t^h)^2 + w_3\omega_t^2$ is running cost which imposes penalties on nozzle's speed and angular rate, and the total spraying time T which is not known apriori and needs to be optimized as well. Additionally, bounds can be imposed on velocity and angular rates: $v_{\min}^x \leq v_t^x \leq v_{\max}^x$, $v_{\min}^h \leq v_t^h \leq v_{\max}^h$ and $\omega_{\min} \leq \omega_t \leq \omega_{\max}$, respectively. This optimal control problem can be solved using model predictive control (MPC), see Chakraborty et al. (2017). However, since typically $N_d \gg 1$ to resolve the surface profile sufficiently, such an approach can be computationally demanding for real time deployment. We explore direct policy search based RL methods which are well suited for such high-dimensional control applications, since they scale gracefully with dimensionality and offer appealing convergence guarantees Peters and Schaal (2008); Kober et al. (2013). However, it is often necessary to carefully choose a specialized policy class to learn the policy in a reasonable number of iterations without getting trapped into poor local optima.

3. Guided Policy Search

Guided policy search (GPS) is a recently proposed direct policy search method which uses a neural network (NN) to parameterize the policy and transforms the policy search into a supervised learning problem, where the training set (which guides the policy search to regions of high reward) is generated by simple trajectory-centric algorithms. NN provide a general and flexible representation which can represent a broad range of behaviors. However, naive supervised learning will often fail

to produce a good policy and a regularized importance sampled policy optimization has been proposed. We will use the end-to-end GPS formulation [Levine et al. \(2016\)](#), which we briefly review. Consider a finite horizon stochastic optimal control problem

$$\min_{\pi_\theta} \mathbb{E}_{\pi_\theta} \left[\sum_{t=1}^T c(\mathbf{s}_t, \mathbf{u}_t) \right], \quad (5)$$

where, $c(\mathbf{s}, \mathbf{u})$ is the cost function, and the expectation \mathbb{E} is taken under the randomized policy $\pi_\theta(\mathbf{u}_t|\mathbf{s}_t)$ which is parameterized by θ and the uncertain system dynamics with state transition probability $p(\mathbf{s}_{t+1}|\mathbf{s}_t, \mathbf{u}_t)$. Let $q(\mathbf{u}_t|\mathbf{s}_t)$ be a guiding policy, then the problem (5) can be reformulated as an equivalent problem:

$$\min_{q, \pi_\theta} \mathbb{E}_q \left[\sum_{t=1}^T c(\mathbf{s}_t, \mathbf{u}_t) \right], \quad q(\mathbf{u}_t|\mathbf{s}_t) = \pi_\theta(\mathbf{u}_t|\mathbf{s}_t), \quad \forall t, \mathbf{s}_t, \mathbf{u}_t. \quad (6)$$

which has an infinite number of constraints. To make the problem tractable one can use the moment matching approach, e.g.

$$\min_{q, \pi_\theta} \mathbb{E}_q \left[\sum_{t=1}^T c(\mathbf{s}_t, \mathbf{u}_t) \right], \quad \mathbb{E}_{q(\mathbf{u}_t|\mathbf{s}_t)q(\mathbf{s}_t)}[\mathbf{u}_t] = E_{\pi_\theta(\mathbf{u}_t|\mathbf{s}_t)q(\mathbf{s}_t)}[\mathbf{u}_t], \quad \forall t. \quad (7)$$

This constrained problem can be solved by a dual descent method, e.g. Bregman Alternative Direction Method of Multipliers (BADMM) Lagrangian formulation leads to

$$\mathcal{L}(q, \pi_\theta) = \sum_{t=1}^T \left[\mathbb{E}_{q(\mathbf{s}_t, \mathbf{u}_t)}(c(\mathbf{s}_t, \mathbf{u}_t)) + \lambda'_{\mu t} (\mathbb{E}_{\pi_\theta(\mathbf{u}_t|\mathbf{s}_t)q(\mathbf{s}_t)}[\mathbf{u}_t] - \mathbb{E}_{q(\mathbf{s}_t, \mathbf{u}_t)}[\mathbf{u}_t]) + \nu_t D_{KL}(q, \pi_\theta) \right],$$

where we have taken the Bregmann divergence to be the KL divergence $D_{KL}(\pi_\theta|q)$. This leads to following iterative optimization scheme,

$$q \leftarrow \arg \min_q \sum_{t=1}^T \left[\mathbb{E}_{q(\mathbf{s}_t, \mathbf{u}_t)}[c(\mathbf{s}_t, \mathbf{u}_t) - \lambda'_{\mu t} \mathbf{u}_t] + \nu_t \phi_t(q, \theta) \right], \quad (8)$$

$$\theta \leftarrow \arg \min_\theta \sum_{t=1}^T \left[\mathbb{E}_{\pi_\theta(\mathbf{u}_t|\mathbf{s}_t)q(\mathbf{s}_t)}[\lambda'_{\mu t} \mathbf{u}_t] + \nu_t \phi_t(\theta, q) \right], \quad (9)$$

$$\lambda_{\mu t} \leftarrow \lambda_{\mu t} + \alpha \nu_t (E_{\pi_\theta(\mathbf{u}_t|\mathbf{s}_t)q(\mathbf{s}_t)}[\mathbf{u}_t] - \mathbb{E}_{q(\mathbf{s}_t, \mathbf{u}_t)}[\mathbf{u}_t]), \quad t = 1, \dots, T, \quad (10)$$

Note that for each $t = 1, \dots, T$, $\lambda_{\mu t}$ is a vector of Lagrangian multiplier with same dimension as the control \mathbf{u}_t . α can be chosen in range $[0, 1]$, lower values lead to better numerical stability. The weights ν_t are initialized to low values such as 0.01 and incremented based on a schedule which adjusts the KL-divergence penalty to keep the policy and trajectory in agreement by roughly the same amount at all time steps. The above steps can be simplified under Gaussian assumptions:

- $\pi_\theta(\mathbf{u}_t|\mathbf{s}_t) \sim \mathcal{N}(\mathbf{u}_t; \mu^\pi(\mathbf{s}_t; \mathbf{w}), \Sigma^\pi)$, where the policy parameters are $\theta = (\mathbf{w}, \Sigma^\pi)$. We will use a neural network (NN) with weights \mathbf{w} to represent the mean policy $\mu^\pi(\mathbf{s}_t; \mathbf{w})$, while Σ^π is policy covariance which is assumed to be state independent,
- $q = \sum_{i=1}^M q_i$ is mixture of Gaussians with $q_i(\mathbf{u}_t|\mathbf{s}_t) \sim \mathcal{N}(\mathbf{u}_t; \mu_t^{q_i}(\mathbf{s}_t), \Sigma_t^{q_i})$

where, $\mathcal{N}(\cdot, \mu, \Sigma)$ is a multinomial normal probability distribution with mean vector μ and covariance matrix Σ . With this assumption, the overall GPS algorithm is summarized below. Steps 1-4 are repeated for a preselected K iterations or else if a prescribed convergence criterion is met.

Step 1: Solve optimization (8) which under the Gaussian assumption simplifies to

$$\arg \min_{q_i} \sum_{t=1}^T \mathbb{E}_{q_i(\mathbf{s}_t, \mathbf{u}_t)} [c_i(\mathbf{s}_t, \mathbf{u}_t) - \mathcal{H}(q_i(\mathbf{u}_t|\mathbf{s}_t))],$$

where, $c_i(\mathbf{s}_t, \mathbf{u}_t) = \frac{c(\mathbf{s}_t, \mathbf{u}_t)}{\nu_t} - \frac{1}{\nu_t} \mathbf{u}_t' \lambda_{\mu t}^i - \log(\pi_{\theta}(\mathbf{u}_t|\mathbf{s}_t))$ and, \mathcal{H} is the standard differential entropy. A local optimal solution (which determines $\mu_t^{q_i}, \Sigma_t^{q_i}$) of the above problem around a selected nominal trajectory can be obtained via a variation of iterative LQR (iLQR) [Li and Todorov \(2004\)](#). The nominal trajectory can be constructed in a variety of ways. e.g. from demonstrations, using randomized control inputs or via solution obtained using MPC [Zhang et al. \(2015\)](#).

Step 2: Sample trajectories $\tau^{ji} = \{(\mathbf{s}_t^{ij}, \mathbf{u}_t^{ij}) : t = 1 : T\}, j = 1, \dots, N$ from

$$q_i(\{\mathbf{s}_1, \mathbf{u}_1, \dots, \mathbf{s}_T, \mathbf{u}_T\}) = p_{i1}(\mathbf{s}_1) \prod_{t=1}^T q_i(\mathbf{u}_t|\mathbf{s}_t) p(\mathbf{s}_{t+1}|\mathbf{s}_t, \mathbf{u}_t). \quad (11)$$

induced by each of the guiding distributions $q_i, i = 1, \dots, M$ with $p_{i1}(\mathbf{s}_1), i = 1, \dots, M$ being the initial state distribution.

Step 3: Train the NN representing the policy mean $\mu^{\pi}(\mathbf{s}; \mathbf{w})$ with a modified objective (9) which under Gaussian assumption becomes:

$$\arg \min_{\mathbf{w}} \frac{1}{2N} \sum_{t=1}^T \sum_{i=1}^M \sum_{j=1}^N \left[\nu_t (\mu_t^{q_i}(\mathbf{s}_t^{ij}) - \mu^{\pi}(\mathbf{s}_t^{ij}; \mathbf{w}))' (\Sigma_t^{q_i})^{-1} (\mu_t^{q_i}(\mathbf{s}_t^{ij}) - \mu^{\pi}(\mathbf{s}_t^{ij}; \mathbf{w})) + 2\lambda_{\mu t}^i \mu^{\pi}(\mathbf{s}_t^{ij}; \mathbf{w}) \right]. \quad (12)$$

The policy covariance Σ^{π} can be computed directly as $\Sigma^{\pi} = \left[\frac{1}{MT} \sum_{i=1}^M \sum_{t=1}^T (\Sigma_t^{q_i})^{-1} \right]^{-1}$.

Step 4: Update the Lagrange multipliers

$$\lambda_{\mu t}^i \leftarrow \lambda_{\mu t}^i + \alpha \nu_t \frac{1}{N} \sum_{j=1}^N [\mu^{\pi}(\mathbf{s}_t^{ij}; \mathbf{w}) - \mu_t^{q_i}(\mathbf{s}_t^{ij})], \quad t = 1, \dots, T; \quad i = 1, \dots, M. \quad (13)$$

3.1. Adaptation of GPS Framework

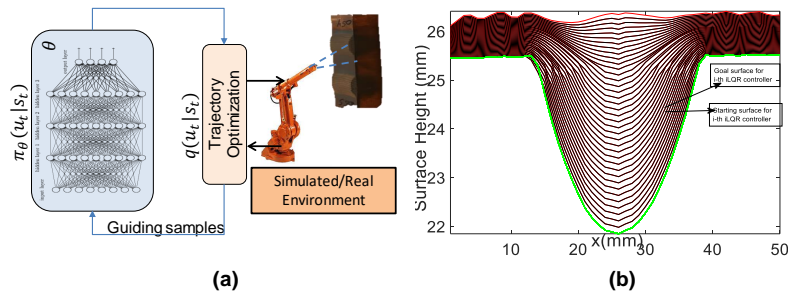


Figure 2: (a) GPS Schematic. (b) Intermediate goals used for generating guiding distributions.

Application of GPS framework to the CS control problem stated in Section 2 required further adaptations. For the selected CS application, achieving the desired profile required multiple passes.

Hence, intermediate goals were defined for computing iLQR based local optimal controllers which will depend on part/defect geometry. Figure 2b shows examples of intermediate goal profiles \mathbf{d}_f^i for the test part considered in our work (see Section 4.1) which were determined so that in each pass least amount of build up happens on the flat portion and maximum deposition occurs in the notch. The objective for the i -th iLQR was to achieve the desired goal profile \mathbf{d}_f^i starting from the previous goal \mathbf{d}_f^{i-1} . Furthermore, the objective function in (4) was modified for each i -th iLQR with this goal profile, and the terminal cost term c_e was absorbed in the total cost leading to $\sum_{t=1}^T (c(\mathbf{s}_t, \mathbf{u}_t) + \|\mathbf{d}_t - \mathbf{d}_f^i\|^2)$. In order to generate training data for NN, initial starting surface for each iLQR was perturbed which not only involved randomized to account for measurement noise in the experiments Tobin et al. (2017), but also included the propagation effect of previous iLQR controller in achieving their goal surface profiles. Generation of rich training sets which covers different possibilities of intermediate states is necessary in sequential decision making tasks: as if NN control actions resulted in surface buildups never encountered in the training, that will further drive the NN to make errors resulting in cascading failure. We will refer to NN controller trained using GPS as GPS based controller (GPSC).

4. Results

4.1. Experimental Setup

The control setup for GPSC demonstration comprised of (see Fig. 3): CS machine/robot, laser displacement sensor (LDS), and standard PC to host the GPSC algorithm. The CS machine comprised of gas heater, powder feeder, and nozzle mounted on a 5-axis robot. A turn table was used to rotate the part to be coated, and thus requiring only a linear motion of nozzle for deposition on the complete surface of an axis symmetric part. The LDS had a 640 pixel resolution with a sampling rate of 1kHz. LABVIEW was used for implementing the control logic which sequentially activated the LDS to provide surface profile measurements, followed by the GPSC code for nozzle speed computation based on the measurements, and then transmitted the nozzle speed commands to the robot controller. For testing the GPSC framework, we used a aluminium cylindrical test coupon with a symmetrical notch representing a defect to be repaired as shown in Fig. 3 b.

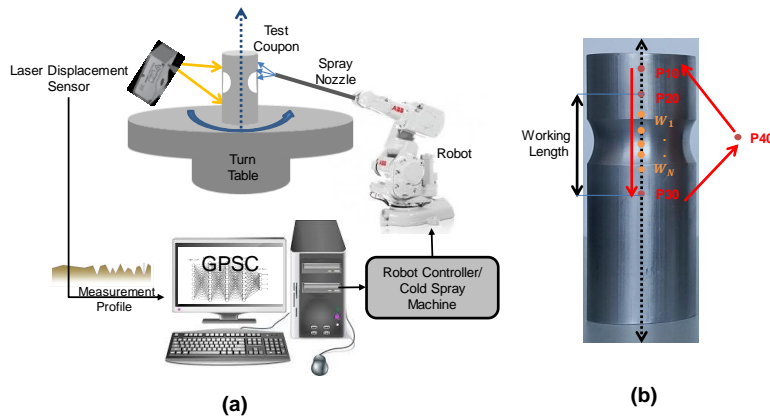


Figure 3: a) Cold spray closed loop experimental setup. b) Cylindrical test coupon with a notch.

4.2. Model Calibration

We used an optimization framework for CS model parameter calibration. The calibration data was generated by making several consecutive passes on the test coupon, where for each pass the speed was held constant taking values $v_i^c \in \{1, 2, 3, 4, 5\}$ mm/sec. The surface profiles after each pass were recorded using the LDS, which we denote by $\mathbf{d}_i, i = 0, \dots, N_c$. Let $\hat{\mathbf{d}}_i(\mathbf{p}; \mathbf{d}_{i-1})$ be predicted surface using the CS model (3) starting with \mathbf{d}_{i-1} , and using parameters \mathbf{p} and constant nozzle speed $\{v_{it}^x = v^c\}_{t=0}^{T_i}$ over the pass. The optimization problem can be defined as (see Fig. 4a)

$$\min_{\mathbf{p}} \sum_{i=1}^{N_c} \|\hat{\mathbf{d}}_i(\mathbf{p}; \mathbf{d}_{i-1}) - \mathbf{d}_i\|^2. \quad (14)$$

We additionally introduced linear constraints $\mathbf{p}_{min} \leq \mathbf{p} \leq \mathbf{p}_{max}$ to bound the parameter values in a desired range. The optimization (14) was solved using fmincon nonlinear optimization routine in MATLAB using a subset of training data, and the remaining set was used for validation. Figure 4b-c shows the calibration results on training and the validation dataset, respectively. The black curves represents experimental data while dotted red curves show calibrated model predictions.

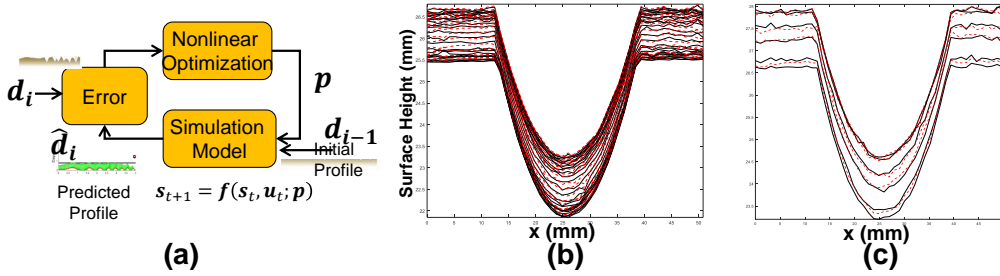


Figure 4: a) Model calibration procedure schematic; b) Calibration results on training data; and c) Calibration results on validation dataset.

4.3. GPSC Deployment

We used the GPSC framework described in Section 3.1, where only the nozzle speed v_t^x was the controlled variable, the nozzle height h_t and orientation α_t were kept fixed. We used $N_d = 100$ for the discretized representation of the surface (see Section 4.1). Consequently, the input layer of the NN consisted of 101 neurons (with one additional input for the nozzle position), and output layer had one neuron corresponding to the nozzle speed. We found that 1 hidden layer with 10 neurons was sufficient for our application. In order to ensure that the output speed remains bounded in range $[0 \ 5]$, we selected a sigmoid activation function for the output layer. The closed loop control was implemented at every pass, i.e. after measurement from LDS was available the controller computed nozzle speed for the entire next pass by propagating the calibrated CS model. This setting of feed-forward/feed-back control is expected to commonly arise in AM applications, where meaningful sensing data may be only available after one or many layers have been deposited. For repetitive spraying, a cyclic robot motion plan was created, which consisted of the two sets of waypoints (see Fig. 3 b): $P_{10}, P_{20}, P_{30}, P_{40}$ are the teach waypoints and remain fixed, while the control waypoints W_1, \dots, W_N depended on the nozzle speed control commands generated by GPSC.

4.4. Findings

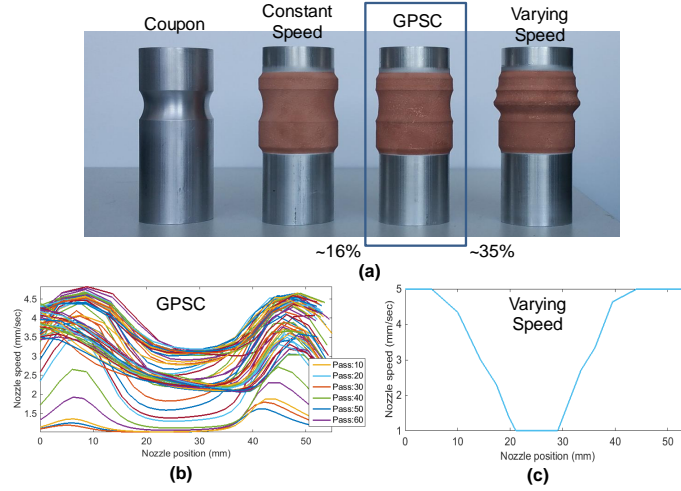


Figure 5: Comparison of different approaches. a) Test coupon after coating, b) Speed profile computed based on GPSC during different passes, c) Hand crafted varying speed profile.

We compare performance of GPSC with two open loop control strategies: constant speed and varying speed. In both these cases the nozzle speed is not changed based on the in-situ LDS measurements. For the constant speed case the speed of nozzle is set to be a constant value of 1mm/sec. For varying speed case the speed changes with nozzle location to prescribed values as shown in Fig. 5c. This speed profile was hand crafted by expert so that nozzle moves fastest in flat portion of coupon resulting in minimal deposition and moves slower in the notch area which requires more deposition. The nozzle speed profiles generated for the different passes during GPSC is shown in the Fig. 5b. Note that GPSC speed profiles are initially similar to the varying speed profile, but adapt as more layers were built to account for various sources of uncertainties/disturbances including robots precision in following the commanded speed, wobbling of the cylinder during rotation, and the variations in powder characteristics. Due to lack of this adaptation in the open loop varying speed case, the final deposit was significantly irregular (see Figure 5a). In fact, GPSC saves 16% scrap material over constant speed, and around 35% over varying speed profile.

5. Conclusions

In this paper we applied guided policy search based RL approach for a high dimensional optimal control problem arising in cold spray manufacturing process. The approach was experimentally validated and showed promising performance. In future, we plan to explore hierarchical RL framework [Barto and Mahadevan \(2003\)](#); [Vezhnevets et al. \(2017\)](#); [Nachum et al. \(2018\)](#) for automatically learning hierarchical structure in additive manufacturing control problems which has a potential to further improve generalization and transfer to different part geometries.

Acknowledgments

Funding provided by UTRC is greatly appreciated.

References

- Andrew G Barto and Sridhar Mahadevan. Recent advances in hierarchical reinforcement learning. *Discrete event dynamic systems*, 13(1-2):41–77, 2003.
- Abhijit Chakraborty, Sergey Shishkin, and Michael J Birnkrant. Optimal control of build height utilizing optical profilometry in cold spray deposits. In *Sensors and Smart Structures Technologies for Civil, Mechanical, and Aerospace Systems 2017*, volume 10168, page 101683H. International Society for Optics and Photonics, 2017.
- Yan Duan, Xi Chen, Rein Houthoofd, John Schulman, and Pieter Abbeel. Benchmarking deep reinforcement learning for continuous control. *CoRR*, abs/1604.06778, 2016. URL <http://arxiv.org/abs/1604.06778>.
- Sarah K Everton, Matthias Hirsch, Petros Stravroulakis, Richard K Leach, and Adam T Clare. Review of in-situ process monitoring and in-situ metrology for metal additive manufacturing. *Materials & Design*, 95:431–445, 2016.
- Jens Kober, J Andrew Bagnell, and Jan Peters. Reinforcement learning in robotics: A survey. *The International Journal of Robotics Research*, 32(11):1238–1274, 2013.
- Sergey Levine and Pieter Abbeel. Learning neural network policies with guided policy search under unknown dynamics. In Z. Ghahramani, M. Welling, C. Cortes, N.D. Lawrence, and K.Q. Weinberger, editors, *Advances in Neural Information Processing Systems 27*, pages 1071–1079. Curran Associates, Inc., 2014.
- Sergey Levine and Vladlen Koltun. Guided policy search. In *Proceedings of the 30th International Conference on Machine Learning, ICML 2013, Atlanta, GA, USA, 16-21 June 2013*, pages 1–9, 2013.
- Sergey Levine and Vladlen Koltun. Learning complex neural network policies with trajectory optimization. In Tony Jebara and Eric P. Xing, editors, *Proceedings of the 31st International Conference on Machine Learning (ICML-14)*, pages 829–837. JMLR Workshop and Conference Proceedings, 2014. URL <http://jmlr.org/proceedings/papers/v32/levine14.pdf>.
- Sergey Levine, Chelsea Finn, Trevor Darrell, and Pieter Abbeel. End-to-end training of deep visuomotor policies. *The Journal of Machine Learning Research*, 17(1):1334–1373, 2016.
- Weiwei Li and Emanuel Todorov. Iterative linear quadratic regulator design for nonlinear biological movement systems. In *ICINCO (1)*, pages 222–229, 2004.
- Timothy P Lillicrap, Jonathan J Hunt, Alexander Pritzel, Nicolas Heess, Tom Erez, Yuval Tassa, David Silver, and Daan Wierstra. Continuous control with deep reinforcement learning. *arXiv preprint arXiv:1509.02971*, 2015.
- Volodymyr Mnih, Koray Kavukcuoglu, David Silver, Andrei A Rusu, Joel Veness, Marc G Belle-mare, Alex Graves, Martin Riedmiller, Andreas K Fidjeland, Georg Ostrovski, et al. Human-level control through deep reinforcement learning. *Nature*, 518(7540):529–533, 2015.
- Volodymyr Mnih, Adria Puigdomenech Badia, Mehdi Mirza, Alex Graves, Timothy Lillicrap, Tim Harley, David Silver, and Koray Kavukcuoglu. Asynchronous methods for deep reinforcement learning. In *International conference on machine learning*, pages 1928–1937, 2016.

- Ofir Nachum, Shixiang Shane Gu, Honglak Lee, and Sergey Levine. Data-efficient hierarchical reinforcement learning. In *Advances in Neural Information Processing Systems*, pages 3303–3313, 2018.
- Jan Peters and Stefan Schaal. Reinforcement learning of motor skills with policy gradients. *Neural networks*, 21(4):682–697, 2008.
- Xinbo Qi, Guofeng Chen, Yong Li, Xuan Cheng, and Changpeng Li. Applying neural-network-based machine learning to additive manufacturing: Current applications, challenges, and future perspectives. *Engineering*, 2019.
- David Silver, Thomas Hubert, Julian Schrittwieser, Ioannis Antonoglou, Matthew Lai, Arthur Guez, Marc Lanctot, Laurent Sifre, Dhharshan Kumaran, Thore Graepel, et al. A general reinforcement learning algorithm that masters chess, shogi, and go through self-play. *Science*, 362(6419):1140–1144, 2018.
- Gustavo Tapia and Alaa Elwany. A review on process monitoring and control in metal-based additive manufacturing. *Journal of Manufacturing Science and Engineering*, 136(6):060801, 2014.
- Josh Tobin, Rachel Fong, Alex Ray, Jonas Schneider, Wojciech Zaremba, and Pieter Abbeel. Domain randomization for transferring deep neural networks from simulation to the real world. In *2017 IEEE/RSJ International Conference on Intelligent Robots and Systems (IROS)*, pages 23–30. IEEE, 2017.
- Alexander Sasha Vezhnevets, Simon Osindero, Tom Schaul, Nicolas Heess, Max Jaderberg, David Silver, and Koray Kavukcuoglu. Feudal networks for hierarchical reinforcement learning. In *Proceedings of the 34th International Conference on Machine Learning-Volume 70*, pages 3540–3549. JMLR. org, 2017.
- Xuemei Wang, Feng Feng, Michael A Klecka, Matthew D Mordasky, Jacquelynn K Garofano, Tahany El-Wardany, Aaron Nardi, and Victor K Champagne. Characterization and modeling of the bonding process in cold spray additive manufacturing. *Additive Manufacturing*, 8:149–162, 2015.
- Shuo Yin, Pasquale Cavaliere, Barry Aldwell, Richard Jenkins, Hanlin Liao, Wenya Li, and Rocco Lupoi. Cold spray additive manufacturing and repair: Fundamentals and applications. *Additive Manufacturing*, 21:628–650, 2018.
- Tianhao Zhang, Gregory Kahn, Sergey Levine, and Pieter Abbeel. Learning deep control policies for autonomous aerial vehicles with mpc-guided policy search. *CoRR*, abs/1509.06791, 2015.